Nano Progress

Ariviyal Publishing

Research Article

DOI: 10.36686/Ariviyal.NP.2021.03.06.031

Nano Prog., (2021) 3(6), 35-47.

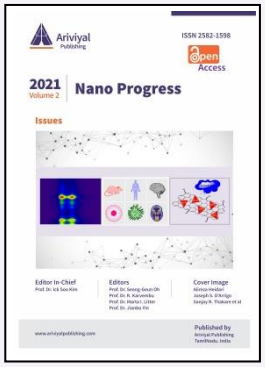

Cadmium Oxide (CdO)–DNA/RNA Sandwiched Complex Composite Plasmonic Nanostructure in Cancer Cells under Synchrotron Radiation

Alireza Heidari*[abcd]

[a]*Faculty of Chemistry, California South University, 14731 Comet St. Irvine, CA 92604, USA.*
[b]*BioSpectroscopy Core Research Laboratory, California South University, 14731 Comet St. Irvine, CA 92604, USA.*
[c]*Cancer Research Institute (CRI), California South University, 14731 Comet St. Irvine, CA 92604, USA.*
[d]*American International Standards Institute, Irvine, CA 3800, USA.*

***Corresponding author E-mail address**: Scholar.Researcher.Scientist@gmail.com; Alireza.Heidari@calsu.us; Central@aisi-usa.org

ISSN: 2582-1598

Crossref

Publication details
Received: 15th June 2021
Revised: 30th July 2021
Accepted: 30th July 2021
Published: 16th August 2021

Abstract: Triptycene Barrelene Anthracene (TBA) is a polycyclic aromatic hydrocarbon consisting of three benzene rings. The name TBA is a composite of phenyl and TBA. In its pure form, it is found in cigarette smoke and is a known irritant, photosensitizing skin and industrial carcinogenic wastewater. Cadmium Oxide (CdO) is an inorganic compound with the formula CdO. It is one of the main precursors to other cadmium compounds. It crystallizes in a cubic rocksalt lattice like sodium chloride, with octahedral cation and anion centers. It occurs naturally as the rare mineral monteponite. CdO can be found as a colorless amorphous powder or as brown or red crystals. CdO is an n–type semiconductor with a band gap of 2.18 eV (2.31 eV) at room temperature (298 K). DNA/RNA, CdO and DNA/RNA–CdO sandwiched complex were characterized by Attenuated Total Reflection–Fourier Transform–Infrared (ATR–FTIR) spectroscopy, Raman spectroscopy, X–Ray Diffraction (XRD) technique and Energy–Dispersive X–Ray (EDAX) spectroscopy. The modified anti–cancer protective membrane was characterized by Scanning Electron Microscope (SEM), EDAX analysis, 3D–Atomic–Force Microscopy (3D–AFM), Transmission Electron Microscopy (TEM) and contact angle analyses and methods. The current study is aimed to use Polysorbate 80 as surfactant for investigating the effectiveness of permeate TBA on the Polyether Ether Ketone (PEEK) anti–cancer protective membrane and the effect of loading DNA/RNA–CdO sandwiched complex on hydrophilicity and anti–cancer properties. The results showed decreasing surface pore size from 227 to 176 and increasing porosity from 101 to 111 with loading DNA/RNA–CdO sandwiched complex, and the permeate of anti–cancer protective membrane increased from 80 to 220 (L/m2.hr.bar) with loading DNA/RNA–CdO sandwiched complex. In addition, the results of current study showed that by increasing DNA/RNA–CdO sandwiched complex nanohybrides to 0.09 Wt% to polymer matrix contact angle decreased from 84.4 to 23 degree. Moreover, the results of current study showed that by increasing DNA/RNA–CdO sandwiched complex nanohybrides to 0.09 Wt% to hydrophilicity of anti–cancer protective membranes increased. All of the above results mentioned fouling of hybride anti–cancer protective membrane decreased than usual form. Therefore, hybride anti–cancer protective membranes of (DNA/RNA–CdO sandwiched complex) with the help of Polysorbate 80 as surfactant may be considered as a suitable anti–cancer protective membrane for treatment of TBA.

Keywords: Elimination; Cancer Cells; Thin Layers; Cadmium Oxide (CdO); Plasmonic Nanostructure; Synchrotron Radiation; Triptycene Barrelene Anthracene (TBA); DNA/RNA; Polyether Ether Ketone (PEEK); Sandwiched Complex; Composite; Anti–Cancer Protective Membrane

1. Introduction

The development of the world with rapid growth of heavy industrial such as food industrial, petrochemical, coal production and pharmaceutical pouring of carcinogenic waste water to river has lot of problem for the world.[1–11] This carcinogenic waste water contains heavy metals, organisms, oils, greases and organic compounds. The organic compounds in carcinogenic waste water are aliphatic, aromatic, Nitrogen Sulfuer Oxygen (NSO) and asphaltens.[12–19] The wide range of contaminants release in to the environment are Polycyclic Aromatic Hydrocarbons (PAHs) such as (Naphthalene, Acenaphthalene, Triptycene Barrelene Anthracene, Banzopyrene etc.). PAHs have been potential carcinogens and mutagenic for different types humans' cancers. Also, it has harmful hazardous for, aquatic animal and plants.[20–34] There is a class of organic pollutant compound containing two or more benzene rings. There are many different methods and techniques for omitting carcinogenic waste water such as low cost adsorption natural materials,[35–37] flotation such as peeling flotation and dissolved air flotation,[38–43] aggregation Zinc silicate and anionic polyacrylamide and polyaluminum Zinc silicate chloride,[44–46] biological treatment and anti–cancer protective membrane separation technology. In view of all above

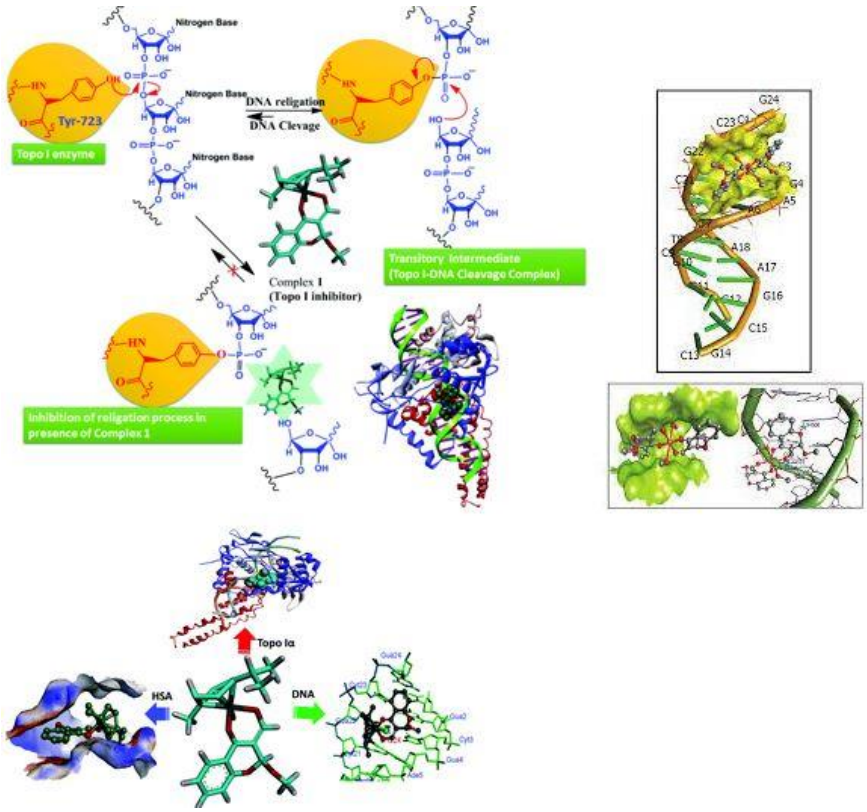

Scheme 1. Schematics of DNA/RNA–thin layers of Cadmium Oxide (CdO) composite plasmonic nanostructure sandwiched complex in a cancer cell.

mentioned methods and techniques, the use of anti–cancer protective membrane separation is an effective technology.

Anti–cancer protective membrane technology is of many advantages such as easy operation, low cost capability of declining pollutants and non–chemical use in operation.[47–49] As a new kind of nanomaterials with three–dimensional (3D) nanostructures, Cadmium (Cd) or Cadmium Oxide (CdO) has recently received a growing research interest. As well known, Cadmium (Cd) or Cadmium Oxide (CdO) that possesses moderate conductivity, large Specific Surface Area (SSA), good chemical stability and also mechanical and anti–cancer properties, can be easily obtained from Cadmium (Cd) by a variety of methods and techniques. Although the super capacitors use of polymer anti–cancer protective membrane by CdO have attention of large group research to self in recent year, several studies reported the use of polyvinylidinedifluride (PVDF), polysulfonefluride (PSF) and polyethersulfone (PES) for the process of removing carcinogenic waste water and dyes. A lot of methods and techniques have been reported to improve properties of polymer anti–cancer protective membrane. Among of all those methods and techniques, blending inorganic oxide particle at casting solution to prepare hybrid anti–cancer protective membrane has lot of attention by researchers. Alireza Heidari et al. were reported the use of inorganic nanoparticles in PEEK anti–cancer protective membrane fabricated from embedding CdO coated and sandwiched with DNA/RNA nanosheets.[50] Scheme 1 shows schematics of DNA/RNA–thin layers of Cadmium Oxide (CdO) composite plasmonic nanostructure sandwiched complex in a cancer cell.

The results were showed that PEEK with DNA/RNA coated and sandwiched by CdO is a good modifier for filtration anti–cancer protective membrane because of high hydrophilicity and improving anti–cancer properties.[50] Alireza Heidari and coworkers, were found that phosphorylated DNA/RNA–CdO sandwiched complex poly sulfone composite anti–cancer protective membrane have potential application to treat carcinogenic waste water because of its good tensile strength and hydrophilicity.[51] Also, Alireza Heidari and his group also were reported a novel Polyether Ether Ketone (PEEK)/Hydrous Manganese Dioxide (HMO). The results of synthesis were the greatest flux recovery and excellent anti–cancer properties among other polymer anti–cancer protective membrane.[51] Sulfated Y–doped Cadmium particle in PEEK were reported by Alireza Heidari and his group as a novel anti–cancer protective membrane which has strong hydrophilicity, antifouling and anti–cancer ability for treating carcinogenic waste water.[51] In this study, Polyether Ether Ketone (PEEK)/Cadmium Oxide (CdO) was synthesized by phase inversion. Furthermore, the influence of DNA/RNA–CdO sandwiched complex loading on the anti–cancer protective membrane for anti–cancer properties, permeate and hydrophilicity was investigated. Moreover, the use of dissolved TBA in water by surfactant (Polysorbate 80) was studied. In addition, operation parameter for efficiency of removal TBA was considered. According to the different investigations, with increasing DNA/RNA–CdO sandwiched complex nanohybrides, hydrophilicity of Mixed Matrix Membrane (MMM) increases while for anti–cancer properties is decreased. The results mentioned DNA/RNA–CdO sandwiched complex anti–cancer protective membrane has been used as suitable anti–cancer protective membrane for treatment of poly aromatic hydrocarbon compound.

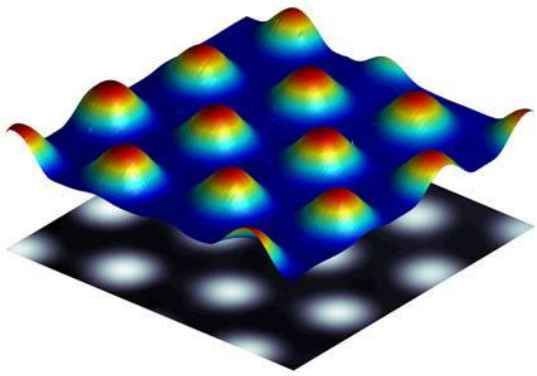

Fig. 1. Molecular structure of DNA/RNA–CdO sandwiched complex.

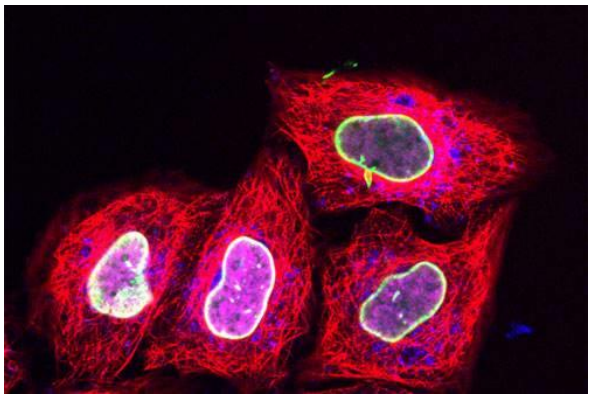

Fig. 2. Molecular structure of DNA/RNA–CdO sandwiched complex.

2. Experimental Methods, Techniques and Materials

2.1. Materials

Powder of Cadmium (99.99%), Sulfuric acid (98%), Sodium nitrate (30%), Hydrogen peroxide (H_2O_2) (30%), Potassium permanganate ($KMnO_4$) and DI water for synthesizing Cadmium Oxide (CdO) were purchased from Sigma–Aldrich Corporation. Tetra Butyl Titanate (TBT), Acetic acid (HAc) and stainless steel autoclave for synthesizing CdO microsphere were also purchased from Sigma–Aldrich Corporation. Polyether Ether Ketone (PEEK) Merck Company, Tetrahydrofuran (THF) as solvents, Polysorbate 80 as surfactant, PEEK as pore former, TBA, which has been listed among the USA EPA priority pollutant, was purchased from Sigma–Aldrich Corporation.

2.2. Preparation of Cadmium Oxide (CdO)–DNA/RNA Sandwiched Complex

Cadmium Oxide (CdO) was prepared from natural Cadmium (Cd) powder according to the different methods and techniques[1,2] and the many procedures which described with some modifications, previously.[1,2] Briefly, 10 (gr) of Cadmium (Cd) was added in to 150 (ml) of Sulfuric acid (98%) while syringed at room temperature for 96 (hr) period. Then, 550 (mg) of Sodium nitrate was added in to the mixture and stirred for 12 (hr). The dispersion was cooled by ice bath. Next, 85 (gr) of $KMnO_4$ was slowly added to the mixture during 90 (min). Afterwards, the mixture of temperature was kept to 20–30 °C while it was stirring for another 6 (hr). The ice bath was removed after 6 (hr). The reaction was followed by adding 250 (ml) of DI water in to the dispersion during 90 (min). Finally, an aqueous solution of H_2O_2 was added to the dispersion. We could have washed DNA/RNA with aqueous HCl until no sulfite ions were found. The pH of solution was remained at 6. Next, the synthesized DNA/RNA was dried at 60 °C for 72 (hr).

2.3. Preparation of Thin Layers of Cadmium Oxide (CdO) Plasmonic Nanostructure

Typically, 10 (ml) of Tetra Butyl Titanate (TBT) was added drop wisely to 150 (ml) of HAc with stirring for 75 (min). After that, the white suspension was obtained. It could transfer to Teflon stainless–steel autoclave. It was heated at 330 °C for 24 (hr). The product was washed by DI water and ethanol. The material was dried at 110 °C for 60 (hr) and after that, calcined at 840 °C for 5 (hr). It was obtained thin layers of CdO plasmonic nanostructure.

2.4. DNA/RNA–CdO Sandwiched Complex Synthesis

DNA/RNA–CdO sandwiched complex was prepared according to the previous reports.[1,2] 75 (mg) of CdO was well dissolved in to 550 (ml) of DI water and then, 840 (mg) of layers of CdO plasmonic nanostructure was added to above solution. After that, it was kept under ultrasonic condition for 20 (hr). Then, it was kept under stirring for 15 (hr). Finally, the mixture was centrifuged and dried for 10 (hr). Molecular structure of DNA/RNA–CdO sandwiched complex and also DAN/RNA–CdO in a human cancer cell are illustrated in the Figs. 1 and 2, respectively.

2.5. Anti–Cancer Properties

The overall porosity of an anti–cancer protective membrane (ε) can be calculated using the gravimetric method as presented in the Eq. (1):

$$\varepsilon = \frac{\omega_1 - \omega_2}{A \times L \times d_w} \quad (1)$$

where ω_1 and ω_2 are the wet and dry weights of the anti–cancer protective membrane, respectively. d_w is the water density (0.998 gr(cm)$^{-3}$), A is the effective area of the anti–cancer protective membrane, a circular anti–cancer protective membrane piece of weighed (W_d) after vacuum drying for 96 (hr) at 50 °C. Then, the anti–cancer protective membrane was immersed in DI water, overnight and weighed (W_w) after the surface was blotted with a filter paper, and the mean pore radius of the anti–cancer protective membrane (r_m) can be calculated using the Guerout–Elford–Ferry Equation (Eq. (2)):

$$r_m = \sqrt{\frac{(2.9 - 1.75\varepsilon) \times 8\eta l Q}{\varepsilon \times A \times \Delta P}} \quad (2)$$

η is the water viscosity (8.9×10^{-4} pas), ΔP is the operation pressure (1 bar), Q is the permeated pure water amount (m^3/s), l is the anti–cancer protective membrane thickness (m) and A is the surface area (m^2).[1,2]

2.6. Anti–Cancer Experiment

The surfactants enhanced solubilization of Hydrophobic Organic Compounds (HOCs) by decreasing the interfacial tension between the contaminants and water.[1,2] 50 (ml) of Polysorbate 80 were placed in 200 (ml) flask. Then, TBA was added to flask more than the required amount to saturate solution. The flask was put on a shaker (1000 rpm, at 27 °C) for 72 (hr) and then, the sample was centrifuged at 10000 (rpm) for 90 (min) to completely un–dissolve the solute. Afterward, the concentration of suspension was determined by UV–Vis spectroscopy.[1,2]

2.6.1. Plasmonic Properties

The anti–cancer protective membrane was first evaluated with pure water flux before using TBA solution. All the anti–cancer protective membranes have effective area 23.273 (cm^2) and each was pressurized at 5 (bar) for period of 45 (min). In order to achieve steady state flux; Pure water flux of anti–cancer protective membrane (J_{w1}) which was evaluated at 5 (bar) could be calculated using Eq. (3):

$$J_{w1} = \frac{V}{A \times t \times \Delta P} \quad (3)$$

where V is the volume of permeate pure water (L), A is the anti–cancer protective membrane effective area in (cm^2), t is permeation flux time (h) and ΔP is the pressure (bar) are used. To determine rejection of anti–cancer protective membrane against crude oil and egg albumin or Bovine Serum Albumin (BSA) the following Equation can be used (Eq. (4)):[1,2]

$$R\% = \left(1 - \frac{C_P}{C_F}\right) \times 100 \quad (4)$$

where C_P and C_F are the concentration of TBA in permeate and feed (mg/l), respectively. The UV–Vis irradiation was used to determine the TBA concentration. In order to obtain Flux Recovery Rate (FRR) of anti–cancer protective membrane, the feed solution tank was refilled with DI water. The pure water flux (J_{w2}) was evaluated to obtain FRR% using Eq. (5):[1,2]

$$FRR = \frac{J_{w2}}{J_{w1}} \times 100 \quad (5)$$

The higher value of FRR, the better antifouling property of the anti–cancer protective membrane.[1,2] Fouling occurs due to the filtration of cake/gel layer on the anti–cancer protective membrane surface. The accumulation of foulants onto the anti–cancer protective membrane pore acts as a driving force for the diffusion of hydrophobic molecules through the anti–cancer protective membrane structure, affecting negatively to both the water permeation and the rejection potential of anti–cancer protective membranes.

2.6.2. Anti–Cancer Protective Membrane

The total fouling resistance of the polymeric anti–cancer protective membrane (RT) is calculated from r_r and r_{ir}. r_r is a reversible fouling ratio which describes the fouling caused by concentration polarization, r_{ir} is an irreversible fouling ratio which describes the fouling caused by adsorption or deposition of protein molecules on the anti–cancer protective membrane surface (Eqs. (6) and (7)):

$$r_r = \frac{J_{w2} - J_P}{J_{w1}} \quad (6)$$

$$r_{ir} = \frac{J_{w1} - J_{w2}}{J_{w1}} \quad (7)$$

R_t is the sum of r_r and r_{ir}, J_{w1} is the permeation water flux (kg/m^2h) (Eq. (8)):

$$J_{w1} = \frac{M}{At} \quad (8)$$

where M is the weight of collected permeate flux, A is the anti–cancer protective membrane effective area, t is the permeation time, J_{w2} is the water flux cleaned anti–cancer protective membrane and J_P is the flux of the BSA solution (Eq. (9)):[1,2]

$$R_t = \left(1 - \frac{J_P}{J_{w1}}\right) \times 100 \quad (9)$$

Under special pressure, after the pure water test, the BSA solutions are immediately replaced in the filtration cell for 360 (min).[1,2]

2.7. Anti–Cancer Protective Membrane Preparation

To prepare Alireza Heidari Solution this shows that cell–derived nanoparticles have been garnering increased attention due to their ability to mimic many of the natural properties displayed by their source cells. This top–down engineering approach can be applied toward the development of novel therapeutic strategies owing to the unique interactions enabled through the retention of complex antigenic information. Herein, we report on the biological functionalization of polymeric nanoparticles with a layer of membrane coating derived from cancer cells. The resulting core–shell nanostructures, which carry the full array of cancer cell membrane antigens, offer a robust platform with applicability toward multiple modes of anticancer therapy. We demonstrate that by coupling the particles with an immunological adjuvant, the resulting formulation can be used to promote a tumor–specific immune response for use in vaccine applications. Moreover, we show that by taking advantage of the inherent homotypic binding phenomenon frequently observed among tumor cells the membrane functionalization allows for a unique cancer targeting strategy that can be utilized for drug delivery applications, predominated DNA/RNA–CdO sandwiched complex was dissolved in Tetrahydrofuran (THF), sonicated at 150°C for 90 (min) and then, dried PEEK polymer. Pellets were added in to the mixture dispersed sufficiently well by stirring until homogenous suspension was obtained. Then, the solution was remained to room temperature for degassing of solution due to 96 (hr). To prepare Mixed Matrix Membrane (MMM), the prepared uniform suspension was poured in to the glass smooth plate and cast by casting blade. Then, the glass plate was immersed in to the deionized water at the room

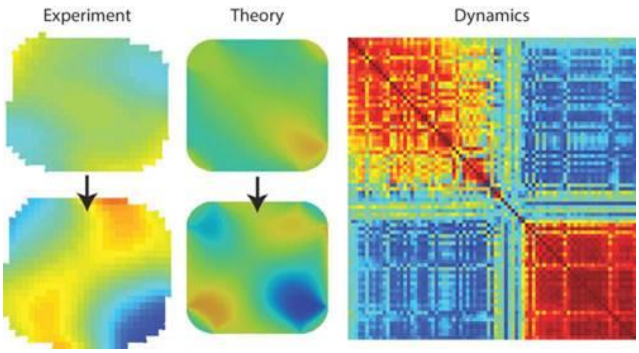

Fig. 3. The glass plate was immersed in to the deionized water at the room temperatures for 96 (hr) to remove solvent and solidify the anti–cancer protective membrane.

temperatures for 96 (hr) to remove solvent and solidify the anti–cancer protective membrane as shown in Fig. 3. The anti–cancer protective membrane thickness was 850 (nm). Addition of 0.55 (gr) nanoparticles to solution is not suitable, the viscosities of solution was very high.

2.8. Characterizations

The structure of DNA/RNA–CdO sandwiched complex was examined by X–Ray Diffraction (XRD), with monochrome Cu Ka radiation. XRD was operated at 85 (KV), 65 (mA). Attenuated Total Reflection–Fourier Transform–Infrared (ATR–FTIR) spectroscopy was used to detect chemical composition of DNA/RNA–CdO sandwiched complex. All samples were recorded in the wave number of 4000–400 (cm^{-1}). Raman spectroscopy is an excellent method to characterize nanomaterials. Energy–Dispersive X–Ray spectroscopy (EDAX) was used to quantify the element content of DNA/RNA–CdO sandwiched complex on the surface of best anti–cancer protective membrane. Transmission Electron Microscopy (TEM), the characterization of synthesized DNA/RNA–CdO sandwiched complex was analyzed by TEM. The DNA/RNA–CdO sandwiched complex anti–cancer protective membrane was dispersed in alcohol. The solution was sonificated for 75 minutes to produce homogenous solution. The suspension was dried in vacuum oven at 135°C. 3D–Atomic–Force Microscopy (3D–AFM) the surface structure and the surface roughness of all anti–cancer protective membranes were measured. The scan was made over an area of 85 (μm) × 10 (μm) to obtain surface roughness and pore size by tapping mode at 135°C. The top surface and cross section of anti–cancer protective membranes were characterized by SEM; the sample was prepared by fracturing the anti–cancer protective membranes in liquid Nitrogen so that the anti–cancer protective membrane was sharply cut. The sample of anti–cancer protective membrane sputters with Gold. Contact angle, using the sessile drop method with a goniometer, hydrophilicity of each anti–cancer protective membrane was measured at 135°C, 75% humidity. 1 (μl) of DI water was carefully dropped on the top surface of anti–cancer protective membrane. The contact angle was equipped with video capture at room temperature. The angle between of water and anti–cancer protective membrane was determined after ten times.

3. Solving Scalar Abraham–Lorentz–Dirac–Langevin (ALDL) Equation for Interaction between Thin Layers of Cadmium Oxide (CdO) Plasmonic Nanostructure and Synchrotron Radiation

We apply the open systems concept and the influence functional formalism introduced in this section to establish a stochastic theory of relativistic moving spinless particles in a quantum scalar field. The stochastic regime resting between the quantum and semi–classical captures the statistical mechanical attributes of the full theory. Applying the particle–centric world–line quantization formulation to the quantum field theory of scalar QED we derive a time–dependent (scalar) Abraham–Lorentz–Dirac–Langevin (ALDL) equation and show that it is the correct semi classical limit for nonlinear particle–field systems without the need of making the dipole or non–relativistic approximations. Progressing to the stochastic regime, we derive multiparticle ALDL equations for nonlinearly coupled particle–field systems. With these equations we show how to address time–dependent dissipation/noise/renormalization in the semi classical and stochastic limits of QED. We clarify the relation of radiation reaction, quantum dissipation and vacuum fluctuations and the role that initial conditions may play in producing non–Lorentz invariant noise. We emphasize the fundamental role of decoherence in reaching the semi classical limit, which also suggests the correct way to think about the issues of runaway solutions and preacceleration from the presence of third derivative terms in the ALDL equation. We show that the semi classical self–consistent solutions obtained in this way are ``paradox'' and pathology free both technically and conceptually. This self–consistent treatment serves as a new platform for investigations into problems related to relativistic moving charges. In fact, we present a stochastic theory of charges moving in an electromagnetic field using non-equilibrium quantum field theory. We give a first principles' derivation of the ALDL equation which depicts the quantum expectation value for a particle's trajectory and its stochastic fluctuations by combining the worldline path integral quantization with the Feynman–Vernon influence functional or closed–time–path effective action methods. At lowest order, the equations of motion are approximated by a stochastic Lorentz–Dirac equation.

Mathematically, the ALDL force is given in SI units by:

$$F_{rad} = \frac{\mu_0 q^2}{6\pi c}\dot{a} = \frac{q^2}{6\pi\varepsilon_0 c^3}\dot{a} \tag{10}$$

or in Gaussian units by:

$$F_{rad} = \frac{2}{3}\frac{q^2}{c^3}\dot{a} \tag{11}$$

Here F_{rad} is the force, $\dot{a}$ is the derivative of acceleration, or the third derivative of displacement), also called jerk, μ_0 is the magnetic constant, ε_0 is the electric constant, c is the speed of light in free space, and q is the electric charge of the particle.

Note that this formula is for non–relativistic velocities; Dirac simply renormalized the mass of the particle in the equation of motion, to find the relativistic version (below).

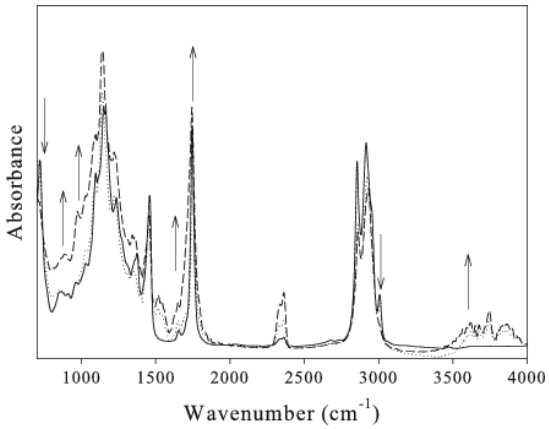

Fig. 4. Attenuated Total Reflection–Fourier Transform–Infrared (ATR–FTIR) spectrums of (a) DNA–CdO (continuous line) and (b) RNA–CdO (dashed line) sandwiched complexes.

Physically, an accelerating charge emits radiation (according to the Larmor formula), which carries momentum away from the charge. Since momentum is conserved, the charge is pushed in the direction opposite the direction of the emitted radiation. In fact, the formula above for radiation force can be derived from the Larmor formula, as shown below.

The simplest derivation for the self–force is found for periodic motion from the Larmor formula for the power radiated from a point charge:

$$P = \frac{\mu_0 q^2}{6\pi c} a^2 \tag{12}$$

If we assume the motion of a charged particle is periodic, then the average work done on the particle by the ALDL force is the negative of the Larmor power integrated over one period from τ_1 to τ_2:

$$\int_{\tau_1}^{\tau_2} F_{rad}.vdt = \int_{\tau_1}^{\tau_2} -Pdt = -\int_{\tau_1}^{\tau_2} \frac{\mu_0 q^2}{6\pi c} a^2 dt = -\int_{\tau_1}^{\tau_2} \frac{\mu_0 q^2}{6\pi c} \frac{dv}{dt}.\frac{dv}{dt} dt \tag{13}$$

The above expression can be integrated by parts. If we assume that there is periodic motion, the boundary term in the integral by parts disappears:

$$\int_{\tau_1}^{\tau_2} F_{rad}.vdt = \frac{\mu_0 q^2}{6\pi c}\frac{dv}{dt}.v\Big|_{\tau_1}^{\tau_2} + \int_{\tau_1}^{\tau_2} \frac{\mu_0 q^2}{6\pi c}\frac{d^2 v}{dt^2}.vdt = -0 + \int_{\tau_1}^{\tau_2} \frac{\mu_0 q^2}{6\pi c}\dot{a}.vdt \tag{14}$$

Clearly, we can identify:

$$F_{rad} = \frac{\mu_0 q^2}{6\pi c}\dot{a} \tag{15}$$

A more rigorous derivation, which does not require periodic motion, was found using an Effective Field Theory formulation. An alternative derivation, finding the fully relativistic expression, was found by Dirac.

Below is an illustration of how a classical analysis can lead to surprising results. The classical theory can be seen to challenge standard pictures of causality, thus signalling either a breakdown or a need for extension of the theory. In this case, the extension is to quantum mechanics and its relativistic counterpart quantum field theory. See the quote from Rohrlich in the introduction concerning "the importance of obeying the validity limits of a physical theory". For a particle in an external force F_{ext}, we have:

$$m\dot{v} = F_{rad} + F_{ext} = mt_0\ddot{v} + F_{ext} \tag{16}$$

Where

$$t_0 = \frac{\mu_0 q^2}{6\pi mc} \tag{17}$$

This equation can be integrated once to obtain:

$$m\dot{v} = \frac{1}{t_0}\int_t^{\infty} exp\left(-\frac{t'-t}{t_0}\right) F_{ext}(t')dt' \tag{18}$$

The integral extends from the present to infinitely far in the future. Thus, future values of the force affect the acceleration of the particle in the present. The future values are weighted by the factor:

$$exp\left(-\frac{t'-t}{t_0}\right) \tag{19}$$

which falls off rapidly for times greater than t_0 in the future. Therefore, signals from an interval approximately t_0 into the future affect the acceleration in the present. For an electron, this time is approximately 10^{-24} sec, which is the time it takes for a light wave to travel across the "size" of an electron, the classical electron radius. One way to define this "size" is as follows: It is (up to some constant factor) the distance r such that two electrons placed at rest at a distance r apart and allowed to fly apart, would have sufficient energy to reach half the speed of light. In other words, it forms the length (or time, or energy) scale where something as light as an electron would be fully relativistic. It is worth noting that this expression does not involve Planck's constant at all, so although it indicates something is wrong at this length scale, it does not directly relate to quantum uncertainty, or to the frequency–energy relation of a photon. Although it is common in quantum mechanics to treat $\hbar \to 0$ as a "classical limit", some speculate that even the classical theory needs renormalization, no matter how Planck's constant would be fixed.

To find the relativistic generalization, Dirac renormalized the mass in the equation of motion with the ALDL force in 1938. This renormalized equation of motion is called the ALDL equation of motion.

The expression derived by Dirac is given in signature $(-,+,+,+)$ by:

$$F_{\mu}^{rad} = \frac{\mu_0 q^2}{6\pi mc}\left[\frac{d^2 p_{\mu}}{d\tau^2} - \frac{p_{\mu}}{m^2 c^2}\left(\frac{dp_v}{d\tau}\frac{dp^v}{d\tau}\right)\right] \tag{20}$$

With Liénard's relativistic generalization of Larmor's formula in the co–moving frame,

$$P = \frac{\mu_0 q^2 \alpha^2 \gamma^6}{6\pi c} \tag{21}$$

one can show this to be a valid force by manipulating the time average equation for power:

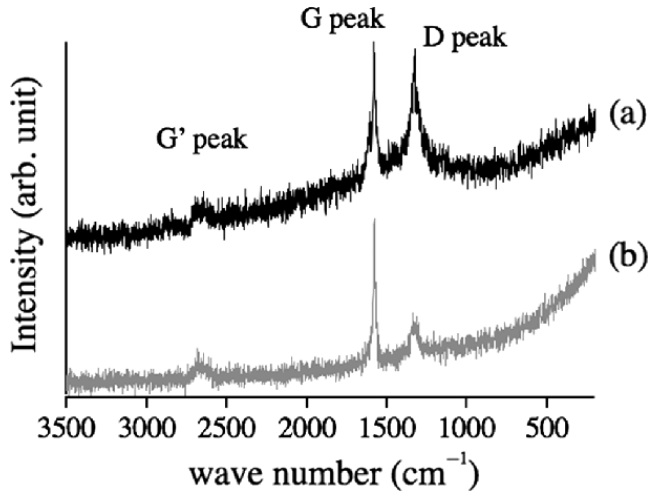

Fig. 5. XRD spectrums of (a) DNA–CdO and (b) RNA–CdO sandwiched complexes.

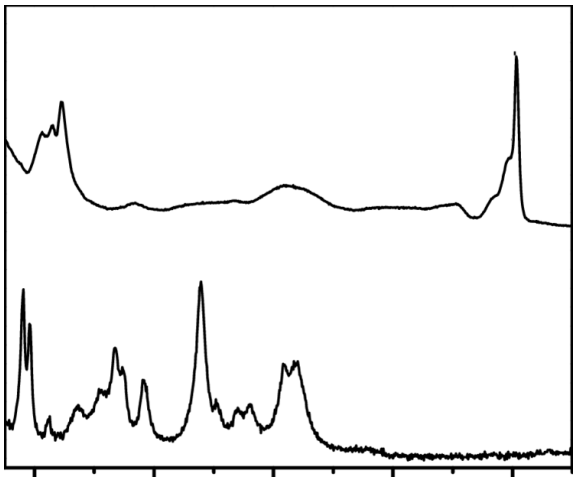

Fig. 6. Raman spectrums of (a) DNA–CdO (upper) and (b) RNA–CdO (lower) sandwiched complexes.

$$\frac{1}{\Delta t}\int_0^t Pdt = \frac{1}{\Delta t}\int_0^t F.vdt \qquad (22)$$

Similar to the non–relativistic case, there are pathological solutions using the ALDL equation that anticipate a change in the external force and according to which the particle accelerates in advance of the application of a force, so–called preacceleration solutions. One resolution of this problem was discussed by Yaghjian, and is further discussed by Rohrlich and Medina.

4. Results and Discussion

4.1. Analysis of ART–FTIR, Raman, XRD and EDAX Spectra

Fig. 4 illustrates the ATR–FTIR spectrum of DNA/RNA–CdO sandwiched complex. In order to obtain the information about functional group of DNA/RNA–CdO sandwiched complex, the ATR–FTIR spectrum of DNA/RNA–CdO sandwiched complex materials were measured and shown in Fig. 4. It was clear that DNA/RNA–CdO sandwiched complex showed many absorption peaks that correspond to various Oxygen functional groups, such as carboxylates or ketones C=O stretching (1777 cm^{-1}), water O–H bending and C≡C stretching (1727 cm^{-1}), C–O stretching (1284 cm^{-1}), C–O stretching of ether group (1227 cm^{-1}) and C–O stretching of epoxide (999 cm^{-1}).[1,2] As for the DNA/RNA–CdO sandwiched complex composite prepared through hydrothermal reaction, the spectrum showed a low absorption–peak intensity of the Oxygen functional groups at 1000–2000 (cm^{-1}) compared to that of DNA/RNA–CdO sandwiched complex. Especially for the peak at 1885 (cm^{-1}) (C=O) of DNA/RNA–CdO sandwiched complex composite, the peak intensity decreased greatly compared to that of DNA/RNA–CdO sandwiched complex. However, the strong peaks at 400–1400 (cm^{-1}) of DNA/RNA–CdO sandwiched complex composite were attributed to the stretching vibration of Cd–O–Cd or Cd–O–DNA/RNA.[1,2] Therefore, the above results confirmed that the formation of DNA/RNA–CdO sandwiched complex composite and chemical interaction strong between surface hydroxyl groups of CdO and functional groups of DNA/RNA.

XRD patterns of DNA/RNA, CdO microsphere and DNA/RNA–CdO sandwiched complex are shown in Fig. 5. The strong peak of DNA/RNA at 2ϑ angle around 27° can be attributed to the reaction between CdO and DNA/RNA sheet in the range of 10°–120°. The diffraction peak at 2ϑ of 15°, 25°, 35°, 45°, 55°, 65°, 75° and 85° are attributed to DNA/RNA–CdO sandwiched complex. DNA/RNA–CdO sandwiched complex shows similar peaks with DNA/RNA–CdO sandwiched complex.[1,2] Fig. 5 shows XRD of DNA/RNA–CdO sandwiched complex at one graph. Raman spectroscopy is one of the most widely used techniques to provide the structural and electronic properties of CdO–based materials.

Raman spectra of DNA/RNA–CdO sandwiched complex were recorded and shown as Fig. 6. The typical four peaks of DNA/RNA–CdO sandwiched complex at 222 (cm^{-1}), 405 (cm^{-1}), 518 (cm^{-1}) and 620 (cm^{-1}) were observed compared with that of DNA/RNA–CdO sandwiched complex, which was ascribed to DNA/RNA–CdO sandwiched complex.[1,2] The strong bands occurred at around 1184 (cm^{-1}) (G band) and 1427 (cm^{-1}) (D band) in DNA/RNA–CdO sandwiched complex composite. The D and G band is common feature for sp^3 and sp^2 in plane vibrations of bonded Carbons.[1,2] The intensity ratio of the D band to the G band usually reflects the order of defects in DNA/RNA–CdO sandwiched complex. The calculated D/G intensity ratios of DNA/RNA–CdO sandwiched complex composite were 0.1123 and 0.4327, respectively. These results agreed well with the results of Alireza Heidari group.[1,2] Moreover, shape, intensity and position of the 2D band of DNA/RNA in the DNA/RNA–CdO sandwiched complex composite can indicate that the single and multi–layer properties of the DNA/RNA sheet.[1,2] From the Raman spectra of DNA/RNA–CdO sandwiched complex composite, we can see that the 2D peak is located at 3150 (cm^{-1}), which shifted to the high wavenumber region compared to that of single–layer DNA/RNA–CdO sandwiched complex (2888 cm^{-1}). We can also see that the peak shape of DNA/RNA in DNA/RNA–CdO sandwiched complex composite is asymmetric compared to symmetric 2D band of single–layer DNA/RNA–CdO sandwiched complex, which indicated that the prepared DNA/RNA–CdO sandwiched complex in the composites was multi–layer. In addition, the G band of DNA/RNA–CdO sandwiched complex is situated at 1774 (cm^{-1}), which shifted to

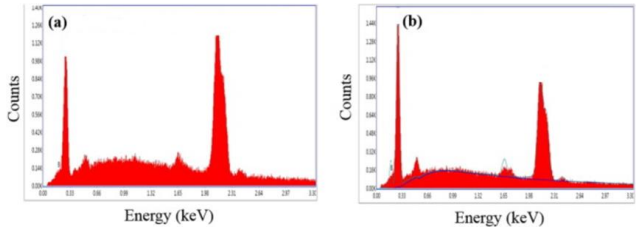

Fig. 7. EDAX spectrums of (a) DNA–CdO and (b) RNA–CdO sandwiched complexes.

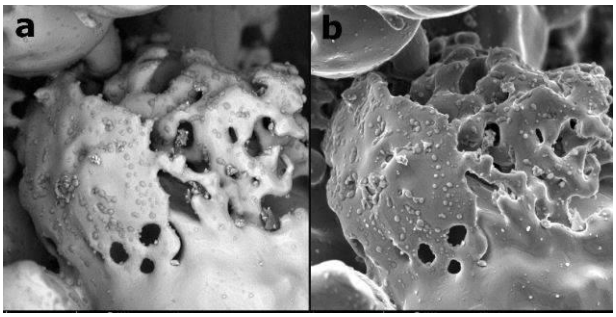

Fig. 8. SEM images of (a) DNA–CdO and (b) RNA–CdO sandwiched complexes.

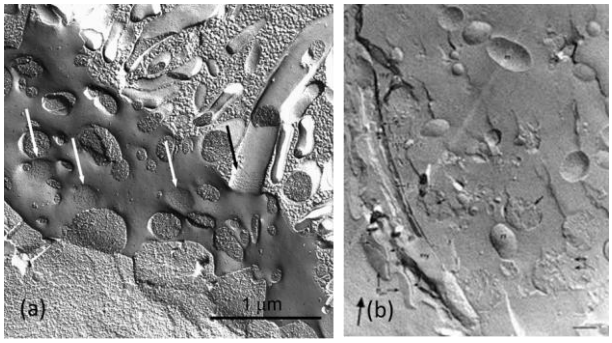

Fig. 9. TEM images of (a) DNA–CdO and (b) RNA–CdO sandwiched complexes.

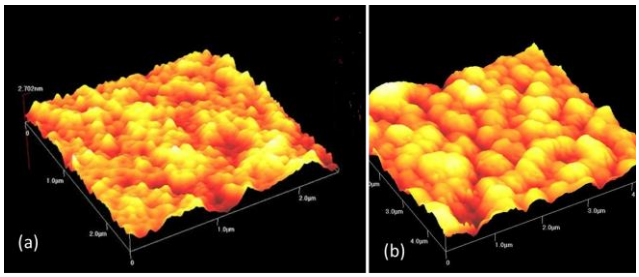

Fig. 10. 3D–AFM images of (a) DNA–CdO and (b) RNA–CdO sandwiched complexes.

high wavenumber region compared to that of single–layer DNA/RNA–CdO sandwiched complex (1660) (cm^{-1}). These results also indicated that the DNA/RNA in the single–layer DNA/RNA–CdO sandwiched complex composite was multi–layer. These results are consistent with the TEM observation (will be explained later in the Fig. 11). However, the ratio of intensity of D/G bands is a measure of the defects present on DNA/RNA–CdO sandwiched complex structure. The DNA/RNA–CdO sandwiched complex band is a result of in–plane vibrations of sp^2 bonded Cadmium atoms whereas the D band is due to out of plane vibrations attributed to the presence of structural defects. Now, when we compare the spectra of DNA/RNA–CdO sandwiched complex together, DNA/RNA–CdO sandwiched complex will have a higher D band. This is due to the disruption of sp^2 bonds of the Cadmium as DNA/RNA–CdO sandwiched complex has oxidative functional groups. Therefore, if the D band is higher, it means that the sp^2 bonds are broken which in turn means that there are more sp^3 bonds. However, D band can be present due to various other reasons. Therefore, if D/G ratio in DNA/RNA–CdO sandwiched complex is higher than DNA/RNA, it means that there are defects. It does not mean that we have more sp^3 than sp^2 in the same sample. In fact, it shows that we have more sp^3 in DNA/RNA–CdO sandwiched complex compared to DNA/RNA.

EDAX of the modified anti–cancer protective membrane is shown in Fig. 7 presence of element on the anti–cancer protective membrane such as Cadmium (Cd), Oxygen (O) and Nitrogen (N). The results show confirms the successful incorporation of DNA/RNA–CdO sandwiched complex in the Mixed Matrix Membrane (MMM).

4.2. Analysis of SEM, TEM and 3D–AFM Images

The surface morphologies of the PEEK anti–cancer protective membranes and the thicknesses of the selective layers were determined by SEM. The images of surface area of anti–cancer protective membrane are shown in Fig. 8. The top surface of anti–cancer protective membrane shows the size of pore decreases when loading of DNA/RNA–CdO sandwiched complexes increases at Mixed Matrix Membrane (MMM). However, by loading of DNA/RNA–CdO sandwiched complexes on the anti–cancer protective membrane, hydrophilicity of anti–cancer protective membrane increases which also indicated by contact angle results.[1,2] The hydrophilicity and the pore size of anti–cancer protective membrane play important roles on separation. Cell membranes with their selective permeability play important functions in the tight control of molecular exchanges between the cytosol and the extracellular environment as the intracellular membranes do within the internal compartments. For this reason, the plasma membranes often represent a challenging obstacle to the intracellular delivery of many anti–cancer molecules. The active transport of drugs through such barrier often requires specific carriers able to cross the lipid bilayer. Cell penetrating peptides (CPPs) are generally 5–30 amino acids long which, for their ability to cross cell membranes, are widely used to deliver proteins, plasmid DNA, RNA, oligonucleotides, liposomes and anti–cancer drugs inside the cells. In this review, we describe the several types of CPPs, the chemical modifications to improve their cellular uptake, the different mechanisms to cross cell membranes and their biological properties upon conjugation with specific molecules. Special emphasis has been given to those with promising application in cancer therapy. The asymmetric anti–cancer protective membrane is ideal for obtaining high permeability, good hydrophilicity and excellent chemical resistance to the feed solution. The cross section of modified anti–cancer protective membrane shows an asymmetric structure. When the MMM is divided to three parts, top surface of anti–cancer protective membrane shows decrease of the pore size anti–cancer protective membrane compares to intermediate and bottom. At the bottom of anti–cancer protective membrane, very large pore size is existed compare to intermediate.

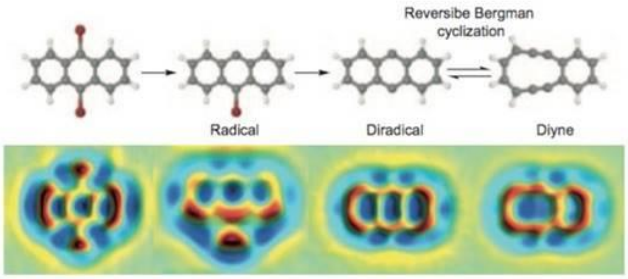

Fig. 11. Schematic and illustration of the nanohybride of DNA/RNA–CdO sandwiched complexes imbedded on polymer PEEK.

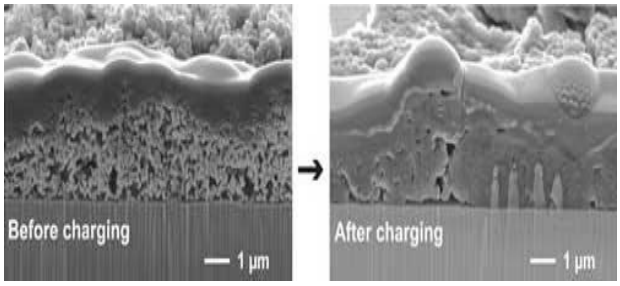

Fig. 12. Permeation flux and rejection of all the anti–cancer protective membrane as function of operation time for cross flow containing 25 (mg/l) TBA.

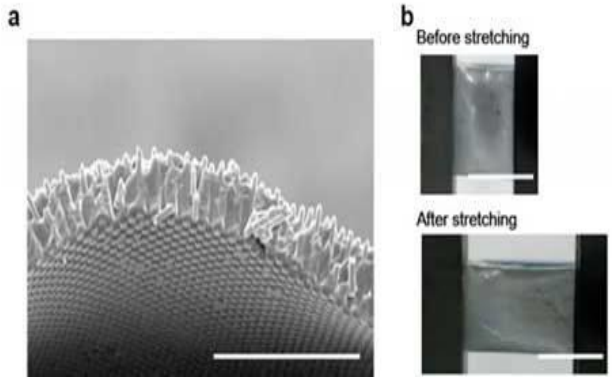

Fig. 13. Permeation flux and rejection of all the anti–cancer protective membrane as function of operation time for cross flow containing 65 (mg/l) TBA.

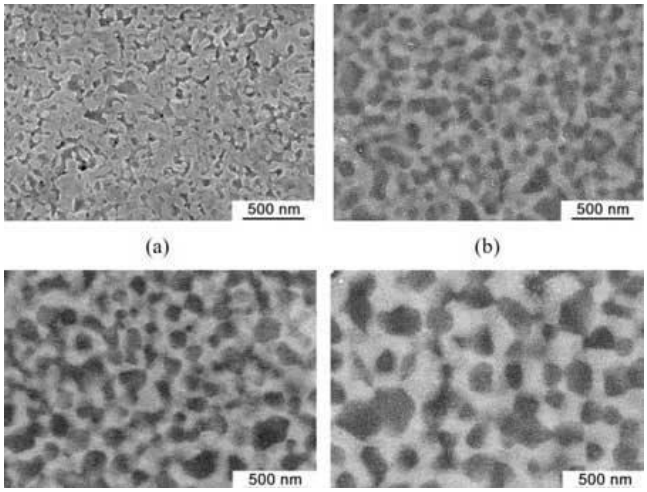

Fig. 14. Sharply decreasing of permeation flux of (0.09 Wt% DNA/RNA–CdO sandwiched complex) anti–cancer protective membrane when increasing concentration of TBA under 0.5 bar at 33 °C (from 15, 25, 35, 45, 55, 65, 75, 85 and 95 (mg/l)).

By increasing nanoparticles, the surface roughness of anti–cancer protective membrane increases and the pore size decreases. The valley and the edges surface MMM become oriented with increase in DNA/RNA–CdO sandwiched complexes nanoparticles and casting bar movement as shown in Figs. 9 and 10. These roughness characteristics can strongly affect the adsorption/desorption of foulants on the anti–cancer protective membrane surface and control the anti–cancer protective membrane fouling. Accordingly, by decreasing the surface roughness of a hydrophilic anti–cancer protective membrane, the trapping of contaminants into the valleys and adhesion at peaks is restricted. The surface of the bare PEEK anti–cancer protective membrane has the lowest roughness and the roughness parameters are increased by the addition of DNA/RNA–CdO sandwiched complexes. Fig. 11 shows the nanohybride of DNA/RNA–CdO sandwiched complexes imbedded on polymer PEEK.

4.3. Experiment for Ultra Anti–Cancer Protective Filtration (UACPF)

4.3.1. Effect of Different Loading DNA/RNA–CdO Sandwiched Complex on Cancer Cells

Figs. 12 and 13 show permeation flux and rejection of all the anti–cancer protective membrane as function of operation time for cross flow containing 25 (mg/l) and 85 (mg/l) PEEK, respectively. The best rejection of PEEK was occurred for 0.09 Wt% DNA/RNA–CdO sandwiched complex. The hybrid anti–cancer protective membrane exhibits higher flux and higher rejection than neat PEEK anti–cancer protective membrane. The main reason for highest hydrophilicity of anti–cancer protective membrane as expressed by the lowest contact angle. Among of all anti–cancer protective membrane PEEK neat exhibit the lowest permeation flux (89 L/m^2.hr.bar) and 0.09 Wt% DNA/RNA–CdO sandwiched complex shows excellent permeation flux 227 (L/m^2.hr.bar). The pores are gradually blocked by adsorption of TBA drop on anti–cancer protective membrane wall which the main cause of formed narrower channel at anti–cancer protective membrane. Then, TBA rejection of PEEK neat anti–cancer protective membrane increases. A good anti–cancer protective membrane should be capable of achieving close to 100% rejection. High rejections are usually accompanied by low permeation fluxes. During fabrication, anti–cancer protective membrane formation process plays an important role and certain factors need proper attention in order to produce a good separation anti–cancer protective membrane. There are several parameters which have been found out to affect the morphology and performance of the prepared anti–cancer protective membrane by phase separation method and technique. Due to the effects of polymer concentration in the casting solution, higher rejection was obtained with denser anti–cancer protective membranes which had thicker skin layers and this resulted in poorer water permeability. On the other hand, the thinner and more porous skin layer anti–cancer protective membranes provided higher water permeability but poorer rejection. According to the contact angle test,[1,2] increasing of nanoparticle weight percentage in anti–cancer protective membrane will increase anti–cancer

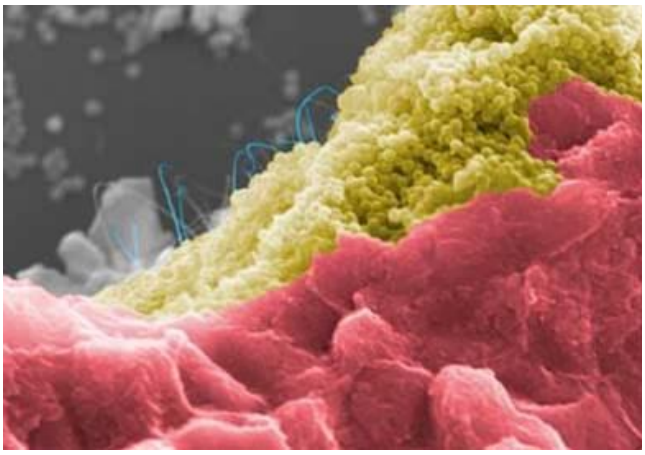

Fig. 15. Effects of Trans–Anti–Cancer–Protective–Membrane Pressure (TACPMP) on the cancer cell.

protective membrane hydrophobicity and consequently, it will increase permeation flux. On the other hand, increasing of nanoparticle weight percentage in anti–cancer protective membrane will increase anti–cancer protective membrane porosity and consequently, it will increase rejection percentage in anti–cancer protective membrane.[1,2]

4.3.2. Effect of Triptycene Barrelene Anthracene (TBA) Concentration on Cancer Cells

Fig. 14 shows sharply decreasing of permeation flux of (0.09 Wt% DNA/RNA–CdO sandwiched complex) anti–cancer protective membrane when increasing concentration of TBA under 0.5 bar at 33°C (from 15, 25, 35, 45, 55, 65, 75, 85 and 95 (mg/l)). In general, temperature increases when matters transform from solid to liquid to gas and to plasma. The temperature of plasma is determined by thermal motions of electrons and heavy particles such as atoms and ions. In the case of a common thermal plasma, when the density of particles is high, due to intensive collisions between eletrons and heavy particles, all particles approach thermal equilibrium.[1] The temperature in such plasma is high, over several thousand degrees.[1] These plasmas are typically used under the atmospheric pressure conditions. On the other hand, if atmospheric pressure plasma discharge is fast, there is another class of plasmas in which electrons and heavy particles are in thermal non–equilibrium. In this case, temperature of the heave particles is much lower than that of the electrons. We shall call these plasmas, cold atmospheric plasmas (CAP). The heavy particle temperature of CAP is between 25°C and 45°C.[2] Such plasmas can be used in biomedicine.[3] Many reactive species including oxygen–based radicals, nitrogen–based radicals, and other components are generated in CAP.[4–6] This complicated chemistry leads to a myriad of interaction between CAP and biological systems including cells and tissues.[7–9] The results showed that PEEK neat anti–cancer protective membrane has more fouling anti–cancer protective membrane. One of the possible reasons for decreasing of flux is concentration of polarization on the surface of anti–cancer protective membrane along the increase of TBA concentration which is the main reason to form gel layer on the anti–cancer protective membrane. Another reason for flux decline is pore blocking owing to impermeability of large drop of TBA. We analyzed the transport of KCl solutions through the bacterial cellulose membrane and Concentration Boundary Layers (CBLs) near membrane with pressure differences on the membrane. The membrane was located in horizontal–plane between two chambers with different KCl solutions. The membrane was located in horizontal–plane between two chambers with different KCl solutions. As results from the elaborated model, gradient of KCl concentration in CBLs is maximal at membrane surfaces in the case when pressure difference on the membrane equals zero. The amplitude of this maximum decreases with time of CBLs buildup. Application of mechanical pressure gradient in the direction of gradient of osmotic pressure on the membrane causes a shift of this maximum into the chamber with lower concentration. In turn, application of mechanical pressure gradient directed opposite to the gradient of osmotic pressure causes the appearance of maximum of concentration gradient in chamber with higher concentration. Besides, the increase of time of CBLs buildup entails a decrease of peak height and shift of this peak further from the membrane. Similar behavior is observed for distribution of energy dissipation in CBLs but for pressure difference on the membrane equal to zero the maximum of energy dissipation is observed in the chamber with lower concentration. We also measured time characteristics of voltage in the membrane system with greater KCl concentrations over the membrane. We can state that mechanical pressure difference on the membrane can suppress or strengthen hydrodynamic instabilities visible as pulsations of measured voltage. Additionally, time of appearance of voltage pulsations, its amplitude, and frequency depend on mechanical pressure differences on the membrane and initial quotient of KCl concentrations in chambers.

4.3.3. Effect of Trans–Anti–Cancer–Protective Membrane Pressure (TACPMP) on Cancer Cells

Fig. 15 shows the effects of Trans–Anti–Cancer–Protective–Membrane Pressure (TACPMP) on the cancer cell. This suggests that when operating pressure gets too high, the anti–cancer protective membrane will be blocked by droplet of pollutant. The formation of gel layer occurs immediately which caused the flux to decline sharply. The anti–cancer protective membrane pores at higher pressure leading to anti–cancer protective membrane fouling at higher rate. These results are consistent with the previous reports.[1,2] The Flux Recovery Rate (FRR) of (0.09 Wt% DNA/RNA–CdO sandwiched complex) decreases from 0.99% to 0.23% with increasing pressure from 1.7 to 2.9.

4.3.4. Hydrophilicity of Mixed Matrix Membrane (MMM) DNA/RNA–CdO Sandwiched Complex in Cancer Cells

Hydrophilicity of PEEK/DNA/RNA–CdO sandwiched complex of each anti–cancer protective membrane measures by contact angle. It is commonly accepted that by increasing the loading of the DNA/RNA–CdO sandwiched complex, the contact angle is decreased and hydrophilicity of anti–cancer protective membrane is indicated higher. According to the reports of Alireza Heidari *et al.*[1,2] the hydroxyl groups of nanoparticles are able to interact with water molecules through Hydrogen bonding and the van der Waals force, which leads to an increase in water permeability.

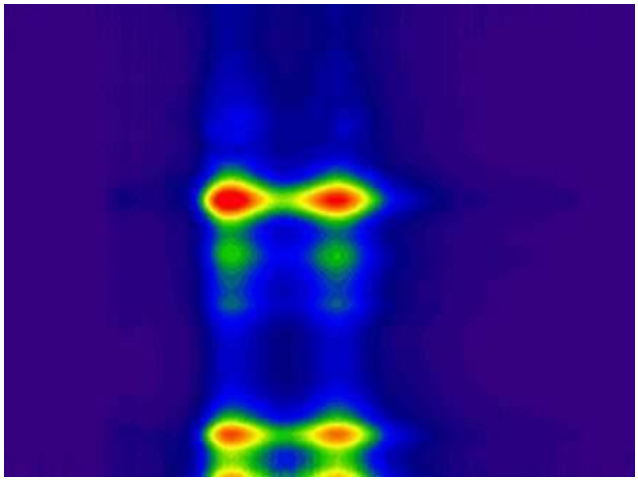

Fig. 16. Hybrid anti–cancer protective membranes such as DNA/RNA–CdO sandwiched complex possess possibility to have a good application in excellent antifouling and anti–cancer abilities and properties.

4.3.5. Anti–Cancer Protective Properties of Mixed Matrix Membrane (MMM)

Anti–cancer protective membrane fouling, as one of the main drawbacks of anti–cancer protective membranes, has various disadvantages such as flux decline, increment of operation cost, maintenance costs and anti–cancer protective membrane degradation. Anti–cancer protective membrane fouling consists of reversible fouling and irreversible fouling, reversible protein or organic material adsorption cause to reversible fouling, which could be removed by hydraulic cleaning. On the contrary, irreversible fouling results of strong adsorption of molecule on the surface or entrapment of pores. The antifouling and anti–cancer properties of anti–cancer protective membrane was calculated from Flux Recovery Ratio (FRR), total fouling rate (R_t), reversible fouling ratio (R_r) and irreversible fouling rate (R_{ir}). As shown in Fig. 16, the R_t were 88, 73, 62% for hybrid anti–cancer protective membrane (DNA/RNA–CdO sandwiched complex) while 59.63% for PEEK neat. The R_r of hybrid anti–cancer protective membranes were decrease from 18, 14, 10 while 49.43 for neat PEEK. The results show hybrid anti–cancer protective membranes had excellent antifouling and anti–cancer ability in PEEK which is possible to have a good application in antifouling for poly aromatic hydrocarbons.

5. Conclusions

In this study, PEEK ultrafiltration anti–cancer protective membranes were prepared by phase inversion with adding different rate nanoparticles DNA/RNA–CdO sandwiched complex. It was used from surfactant Polysorbate 80 for increasing solubility of TBA in water. The current study investigated effects of nanoparticles on permeate hydrophilicity and antifouling of PEEK on the anti–cancer protective membrane. Many reasons that make of DNA/RNA a suitable material to combine with CdO and used to make polymer anti–cancer protective membrane. DNA/RNA provides a way to enhance the separation between the electron and the hole also increase the absorption range, including at the visible region. The new simple theoretical model of DNA/RNA for the interface exciton with an itinerant photo–excited hole is already studied.[1,2] The main parameter of the model is the separation *d* between electron and hole, which are assumed to be conned in the two planes. By variational numerical calculation, we obtain the values of main parameters of the exciton: binding energies, effective Bohr radius, and oscillator strengths versus parameter *d*. Checking the applicable of the model, we find good agreement with the previous obtained results.[1,2] We find also a strong dependence on the separation *d* and an existence of the "death region" of the exciton coursed by the hole band gap potential. Finally, they also increase the interaction area and adsorption of pollutants and dyes with the photocatalyser by creating a π–π interaction. By increasing of DNA/RNA–CdO sandwiched complex nanohybrids increasing of hydrophilicity of MMM. The permeation flux of 100 (mg/l) PEEK was increased by increasing of the nanoparticles which shows in anti–cancer protective membrane contact angle test. Also, by increasing of the nanoparticles in anti–cancer protective membrane increasing of roughness and decreasing of pore size of MMM. Therefore, the MMM (0.09 Wt %) with good rejection and low antifouling will be potentially useful for treatment of the water pollutant with PAHs.

Acknowledgements

This study was supported by the Cancer Research Institute (CRI) Project of Scientific Instrument and Equipment Development, the National Natural Science Foundation of the United Sates, the International Joint BioSpectroscopy Core Research Laboratory Program supported by the California South University (CSU), and the Key project supported by the American International Standards Institute (AISI), Irvine, California, USA.

Conflicts of Interest

The authors declare no conflict of interest.

References

1 Heidari A.; Brown C. Study of Composition and Morphology of Cadmium Oxide (CdO) Nanoparticles for Eliminating Cancer Cells. *J. Nanomed. Res*., 2015, **2**, 20 Pages. [CrossRef]

2 Heidari A.; Brown C. Study of Surface Morphological, Phytochemical and Structural Characteristics of Rhodium (III) Oxide (Rh_2O_3) Nanoparticles. *Int. J. Pharmacol. Phytochem. Ethnomed*., 2015, **1**, 15-19. [CrossRef]

3 Heidari A. An Experimental Biospectroscopic Study on Seminal Plasma in Determination of Semen Quality for Evaluation of Male Infertility. *Int J. Adv. Technol.,* 2016, **7**, 1-2. [CrossRef]

4 Heidari A. Extraction and Preconcentration of N–tolyl–sulfonyl–Phosphoramid–saeure–dichlorid as an Anti–cancer Drug from Plants: A Pharmacognosy Study. *J. Pharmacogn. Nat. Prod*., 2016, **2**, e103. [CrossRef]

5 Heidari A. A Thermodynamic Study on Hydration and Dehydration of DNA and RNA– Amphiphile Complexes. *J. Bioeng. Biomed. Sci. S*, 2016, 6. [Link]

6 Heidari A. Computational Studies on Molecular Structures and Carbonyl and Ketene Groups' Effects of Singlet and Triplet Energies of

Azidoketene O= C= CH–NNN and Isocyanatoketene O= C= CH–N= C= O. *J. Appl. Computat. Math*., 2016, **5**, e142. [CrossRef]

7 Heidari A. Study of Irradiations to Enhance the Induces the Dissociation of Hydrogen Bonds between Peptide Chains and Transition from Helix Structure to Random Coil Structure Using ATR–FTIR, Raman and ^{1}HNMR Spectroscopies. *J. Biomol. Res. Ther*., 2016, **5**, e146. [CrossRef]

8 Heidari A. Future Prospects of Point Fluorescence Spectroscopy, Fluorescence Imaging and Fluorescence Endoscopy in Photodynamic Therapy (PDT) for Cancer Cells. *J. Bioanal. Biomed*., 2016, **8**, e135. [CrossRef]

9 Heidari A. A Bio–Spectroscopic Study of DNA Density and Color Role as Determining Factor for Absorbed Irradiation in Cancer Cells. *Adv. Cancer Prev.*, 2016, **1**, e102. [CrossRef]

10 Heidari A. Manufacturing Process of Solar Cells Using Cadmium Oxide (CdO) and Rhodium (III) Oxide (Rh_2O_3) Nanoparticles. *J. Biotechnol. Biomater*., 2016, **6**, e125. [CrossRef]

11 Heidari A. A Novel Experimental and Computational Approach to Photobiosimulation of Telomeric DNA/RNA: A Biospectroscopic and Photobiological Study. *J. Res. Development*, 2016, **4**, 1000144. [CrossRef]

12 Heidari A. Biochemical and Pharmacodynamical Study of Microporous Molecularly Imprinted Polymer Selective for Vancomycin, Teicoplanin, Oritavancin, Telavancin and Dalbavancin Binding. *Biochem Physiol*., 2016, **5**, e146. [CrossRef]

13 Heidari A. Anti–Cancer Effect of UV Irradiation at Presence of Cadmium Oxide (CdO) Nanoparticles on DNA of Cancer Cells: A Photodynamic Therapy Study. *Arch. Cancer Res.*, 2016, **4**, 14. [CrossRef]

14 Heidari A. Biospectroscopic Study on Multi–Component Reactions (MCRs) in Two A–type and B–type Conformations of Nucleic Acids to Determine Ligand Binding Modes, Binding Constant and Stability of Nucleic Acids in Cadmium Oxide (CdO) Nanoparticles–Nucleic Acids Complexes as Anti–Cancer Drugs. *Arch. Cancer Res*., 2016, **4**, 65. [CrossRef]

15 Heidari A. Simulation of Temperature Distribution of DNA/RNA of Human Cancer Cells using Time–Dependent Bio–Heat Equation and Nd: YAG Lasers. *Arch. Cancer Res*., 2016, **4**, 69. [CrossRef]

16 Heidari A. Quantitative Structure–Activity Relationship (QSAR) Approximation for Cadmium Oxide (CDO) and Rhodium (iii) Oxide (RH_2O_3) Nanoparticles as Anti–Cancer Drugs for the Catalytic Formation of Proviral DNA from Viral RNA using Multiple Linear and Non–linear Correlation Approach. *Ann. Clin. Lab. Res*., 2016, **4**, 76. [CrossRef]

17 Heidari A. Biomedical Study of Cancer Cells DNA Therapy using Laser Irradiations at Presence of Intelligent Nanoparticles. *J. Biomedical Sci*., 2016, **5**, 9. [CrossRef]

18 Heidari A. Measurement the Amount of Vitamin D2 (ergocalciferol), vitamin D3 (cholecalciferol) and Absorbable Calcium (Ca^{2+}), Iron (II)(Fe^{2+}), Magnesium (Mg^{2+}), Phosphate (PO^{4-}) and Zinc (Zn^{2+}) in Apricot using High–Performance Liquid Chromatography (HPLC) and Spectroscopic Techniques. *J. Biom. Biostat*., 2016, **7**, 292. [CrossRef]

19 Heidari A. Spectroscopy and Quantum Mechanics of the Helium Dimer (He_2^+), Neon Dimer (Ne_2^+), Argon Dimer (Ar_2^+), Krypton Dimer (Kr_2^+), Xenon Dimer (Xe_2^+), Radon Dimer (Rn_2^+) and Ununoctium Dimer (Uuo_2^+) Molecular Cations. *Chem. Sci. J*., 2016, **7**, e112. [CrossRef]

20 Heidari A. Human Toxicity Photodynamic Therapy Studies on DNA/RNA Complexes as a Promising New Sensitizer for the Treatment of Malignant Tumors using Bio–Spectroscopic Techniques. *J. Drug Metab. Toxicol*., 2016, **7**, e129. [CrossRef]

21 Heidari A. Novel and Stable Modifications of Intelligent Cadmium Oxide (Cdo) Nanoparticles as Anti–Cancer Drug in Formation of Nucleic Acids Complexes for Human Cancer Cells' Treatment. *Biochem. Pharmacol*. (Los Angel), 2016, **5**, 207. [CrossRef]

22 Heidari A. A Combined Computational and QM/MM Molecular Dynamics Study on Boron Nitride Nanotubes (BNNTs), Amorphous Boron Nitride Nanotubes (a–BNNTs) and Hexagonal Boron Nitride Nanotubes (h–BNNTs) as Hydrogen Storage. *Struct. Chem. Crystallogr. Commun*., 2016, **2**, 7. [CrossRef]

23 Heidari A. Pharmaceutical and Analytical Chemistry Study of Cadmium Oxide (CdO) Nanoparticles Synthesis Methods and Properties as Anti–Cancer Drug and its Effect on Human Cancer Cells. *Pharm. Anal. Chem.* Open Access 2: 113. *J. Biomedical Sci*., 2016, **5**, 21. [CrossRef]

24 Heidari A. A Chemotherapeutic and Biospectroscopic Investigation of the Interaction of Double–Standard DNA/RNA–Binding Molecules with Cadmium Oxide (CdO) and Rhodium (III) Oxide (Rh_2O_3) Nanoparticles as Anti–Cancer Drugs for Cancer Cells' Treatment. *Chemo. Open Access*, 2016, **5**, e129. [CrossRef]

25 Heidari A. Pharmacokinetics and Experimental Therapeutic Study of DNA and Other Biomolecules Using Lasers: Advantages and Applications. *J. Pharmacokinet. Exp. Ther*., 2016, **1**, e005. [CrossRef]

26 Heidari A. Determination of Ratio and Stability Constant of DNA/RNA in Human Cancer Cells and Cadmium Oxide (CdO) Nanoparticles Complexes Using Analytical Electrochemical and Spectroscopic Techniques. *Insights Anal. Electrochem*., 2016, **2**, 14. [CrossRef]

27 Heidari A. Discriminate Between Antibacterial and Non–Antibacterial Drugs Artificial Neutral Networks of a Multilayer Perceptron (MLP) Type Using a Set of Topological Descriptors. *J. Heavy Met. Toxicity Dis*., 2016, **1**, 28. [CrossRef]

28 Heidari A. Combined Theoretical and Computational Study of the Belousov–Zhabotinsky Chaotic Reaction and Curtius Rearrangement for Synthesis of Mechlorethamine, Cisplatin, Streptozotocin, Cyclophosphamide, Melphalan, Busulphan and BCNU as Anti–Cancer Drugs. *Insights Med. Phys*., 2016, **1**, 7. [CrossRef]

29 Heidari A. A Translational Biomedical Approach to Structural Arrangement of Amino Acids' Complexes: A Combined Theoretical and Computational Study. *Transl. Biomed*., 2016, **7**, 72. [CrossRef]

30 Heidari A. Ab Initio And Density Functional Theory (DFT) Studies of Dynamic Nmr Shielding Tensors and Vibrational Frequencies of DNA/RNA and Cadmium Oxide (Cdo) Nanoparticles Complexes in Human Cancer Cells. *J. Nanomedine Biotherapeutic. Discov*., 2016, **6**, e144. [CrossRef]

31 Heidari A. Molecular Dynamics and Monte–Carlo Simulations for Replacement Sugars in Insulin Resistance, Obesity, LDL Cholesterol, Triglycerides, Metabolic Syndrome, Type 2 Diabetes and Cardiovascular Disease: A Glycobiological Study. *J. Glycobiol*., 2016, **5**, e111. [CrossRef]

32 Heidari A. Synthesis and Study of 5–[(Phenylsulfonyl) Amino]–1, 3, 4–Thiadiazole–2–Sulfonamide as Potential Anti–Pertussis Drug Using Chromatography and Spectroscopy Techniques. *Transl. Med*. (Sunnyvale), 2016, **6**, e137. [CrossRef]

33 Heidari A. Nitrogen, Oxygen, Phosphorus and Sulphur Heterocyclic Anti–Cancer Nano Drugs Separation in the Supercritical Fluid of Ozone (O_3) using Soave–Redlich–Kwong (SRK) and Pang–Robinson (PR) Equations. *Electronic J. Biol*., 2016, **12**, 300-301. [CrossRef]

34 Heidari A. An Analytical and Computational Infrared Spectroscopic Review of Vibrational Modes in Nucleic Acids. *Austin J. Anal. Pharm. Chem*., 2016, **3**, 1058. [CrossRef]

35 Heidari A.; Brown C. Phase, Composition and Morphology Study and Analysis of Os–Pd/Hfc Nanocomposites. *Nano Res. Appl*., 2016, **2**, 14. [CrossRef]

36 Heidari A.; Brown C. Vibrational Spectroscopic Study of Intensities and Shifts of Symmetric Vibration Modes of Ozone Diluted by Cumene. *Int. J. Adv. Chem*., 2016, **4**, 5-9. [CrossRef]

37 Heidari A. Study of the Role of Anti–Cancer Molecules with Different Sizes for Decreasing Corresponding Bulk Tumor Multiple Organs or Tissues. *Arch. Can. Res*., 2016, **4**, 38. [Link]

38 Heidari A. Genomics and Proteomics Studies of Zolpidem, Necopidem, Alpidem, Saripidem, Miroprofen, Zolimidine, Olprinone and Abafungin as Anti–Tumor, Peptide Antibiotics, Antiviral and Central Nervous System (CNS) Drugs. *J. Data Mining Genomics & Proteomics*, 2016, **7**, e125. [CrossRef]

39 Heidari A. Pharmacogenomics and Pharmacoproteomics Studies of Phosphodiesterase–5 (Pde5) Inhibitors and Paclitaxel Albumin–Stabilized Nanoparticles as Sandwiched Anti–Cancer Nano Drugs between Two Dna/Rna Molecules of Human Cancer Cells. *J. Pharmacogenomics Pharmacoproteomics*, 2016, **7**, e153. [CrossRef

40 Heidari A. Biotranslational Medical and Biospectroscopic Studies of Cadmium Oxide (Cdo) Nanoparticles–Dna/Rna Straight and Cycle Chain Complexes as Potent Anti–Viral, Anti–Tumor and Anti–Microbial Drugs: A Clinical Approach. *Transl. Biomed*., 2016, **7**, 76. [Link]

41 Heidari A. A Comparative Study on Simultaneous Determination and Separation of Adsorbed Cadmium Oxide (Cdo) Nanoparticles on Dna/Rna of Human Cancer Cells using Biospectroscopic Techniques and Dielectrophoresis (Dep) Method. *Arch. Can. Res*., 2016, **4**, 42. [Link]

42 Heidari A. Cheminformatics and System Chemistry of Cisplatin, Carboplatin, Nedaplatin, Oxaliplatin, Heptaplatin and Lobaplatin as Anti–Cancer Nano Drugs: A Combined Computational and Experimental Study. *J. Inform. Data Min*., 2016, **1**, 3. [Link]
43 Heidari A. Linear and Non–Linear Quantitative Structure–Anti–Cancer–Activity Relationship (QSACAR) Study of Hydrous Ruthenium (IV) Oxide (RuO_2) Nanoparticles as Non–Nucleoside Reverse Transcriptase Inhibitors (NNRTIs) and Anti–Cancer Nano Drugs. *J. Integr. Oncol*., 2016, **5**, e110. [CrossRef]
44 Heidari A. Synthesis, Characterization and Biospectroscopic Studies of Cadmium Oxide (CdO) Nanoparticles–Nucleic Acids Complexes Absence of Soluble Polymer as a Protective Agent Using Nucleic Acids Condensation and Solution Reduction Method. *J. Nanosci. Curr. Res*., 2016, **1**, e101. [CrossRef]
45 Heidari A. Coplanarity and Collinearity Of 4'–Dinonyl–2, 2'–Bithiazole in One Domain of Bleomycin and Pingyangmycin to be Responsible for Binding of Cadmium Oxide (Cdo) Nanoparticles to DNA/RNA Bidentate Ligands as Anti–Tumor Nano Drug. *Int. J. Drug Dev. Res.*, 2016, **8**, 007-008. [Link]
46 Heidari A. A Pharmacovigilance Study on Linear and Non–Linear Quantitative Structure (Chromatographic) Retention Relationships (QSRR) Models for the Prediction of Retention Time of Anti–Cancer Nano Drugs under Synchrotron Radiations. *J. Pharmacovigil*., 2016, 4, e161. [CrossRef]
47 Heidari A. Nanotechnology in Preparation of Semipermeable Polymers. *J. Adv. Chem. Eng*., 2016, **6**, 157. [Link]
48 Heidari A. A Gastrointestinal Study on Linear and Non–Linear Quantitative Structure (Chromatographic) Retention Relationships (QSRR) Models for Analysis 5–Aminosalicylates Nano Particles as Digestive System Nano Drugs Under Synchrotron Radiations. *J. Gastrointest. Dig. Syst*., 2016, **6**, e119. [Link]
49 Heidari A. DNA/RNA Fragmentation and Cytolysis in Human Cancer Cells Treated with Diphthamide Nano Particles Derivatives. *Biomedical Data Mining*, 2016, **5**, e102. [Link]
50 Heidari A. A Successful Strategy for the Prediction of Solubility in the Construction of Quantitative Structure–Activity Relationship (QSAR) and Quantitative Structure–Property Relationship (QSPR) under Synchrotron Radiations using Genetic Function Approximation (GFA) Algorithm. *J. Mol. Biol. Biotechnol*., 2016, **1**, 1. [Link]
51 Heidari A. Computational Study on Molecular Structures of C_{20}, C_{60}, C_{240}, C_{540}, C_{960}, C_{2160} and C_{3840} Fullerene Nano Molecules under Synchrotron Radiations using Fuzzy Logic. *J. Material Sci. Eng*., 2016, **5**, 282. [CrossRef]